New Journal of Physics
The open-access journal for physics

Differential cross sections for non-sequential double ionization of He by 52 eV photons from the Free Electron Laser in Hamburg, FLASH

M Kurka[1,2,13], J Feist[3,4], D A Horner[5], A Rudenko[1,2], Y H Jiang[1], K U Kühnel[1], L Foucar[1,2], T N Rescigno[6], C W McCurdy[6,7], R Pazourek[3], S Nagele[3], M Schulz[8], O Herrwerth[9], M Lezius[9], M F Kling[9], M Schöffler[6], A Belkacem[6], S Düsterer[10], R Treusch[10], B I Schneider[11,12], L A Collins[5], J Burgdörfer[3], C D Schröter[1], R Moshammer[1] and J Ullrich[1,2]

[1] Max-Planck-Institut für Kernphysik, 69117 Heidelberg, Germany
[2] Max-Planck Advanced Study Group at CFEL, 22607 Hamburg, Germany
[3] Institute for Theoretical Physics, Vienna University of Technology, 1040 Vienna, Austria, EU
[4] ITAMP, Harvard-Smithsonian Center for Astrophysics, Cambridge, MA 02138, USA
[5] Los Alamos National Laboratory, Theoretical Division, Los Alamos, NM 87545, USA
[6] Lawrence Berkeley National Laboratory, Chemical Sciences and Ultrafast X-ray Science Laboratory, Berkeley, CA 94720, USA
[7] Departments of Applied Science and Chemistry, University of California, Davis, CA 95616, USA
[8] Missouri University of Science and Technology, Physics Department and LAMOR, Rolla, MO 65409, USA
[9] Max-Planck-Institut für Quantenoptik, 85748 Garching, Germany
[10] DESY, 22607 Hamburg, Germany
[11] Office of Cyberinfrastructure/Physics Division, National Science Foundation, Arlington, VA 22230, USA
[12] Electron and Optical Physics Division, National Institute of Standards and Technology, Gaithersburg, MD 20899, USA
E-mail: moritz.kurka@mpi-hd.mpg.de

New Journal of Physics **12** (2010) 073035 (17pp)
Received 6 May 2010
Published 27 July 2010
Online at http://www.njp.org/
doi:10.1088/1367-2630/12/7/073035

[13] Author to whom any correspondence should be addressed.

Abstract. Two-photon double ionization of He is studied at the Free Electron Laser in Hamburg (FLASH) by inspecting He^{2+} momentum ($\vec{P}(He^{2+})$) distributions at 52 eV photon energy. We demonstrate that recoil ion momentum distributions can be used to infer information about highly correlated electron dynamics and find the first experimental evidence for 'virtual sequential ionization'. The experimental data are compared with the results of two calculations, both solving the time-dependent Schrödinger equation. We find good overall agreement between experiment and theory, with significant differences for cuts along the polarization direction that cannot be explained by the experimental resolution alone.

Contents

1. Introduction

The interaction of a 'few' photons with a 'few' electrons in atoms and molecules (clusters, solids) constitutes one of the most fundamental nonlinear reactions occurring when intense extreme ultraviolet (EUV), vacuum ultraviolet (VUV) or x-radiation meets matter. Free electron lasers (FELs), such as the Free Electron Laser in Hamburg (FLASH) [1], the Japanese SCSS test facility at Spring 8 [2] and, most recently, LCLS at SLAC in Stanford [3] now deliver such radiation routinely for a broad spectrum of scientific applications. In addition, high-power visible laser-based sources have been demonstrated to produce intense high-harmonic (HH) radiation in the EUV regime [4]. Therefore, a detailed understanding of *nonlinear few-electron quantum dynamics* is not only of fundamental scientific importance but also of considerable practical relevance for research on FELs in general. Such reactions essentially underlie all radiation–matter interactions in any experiment at typical FEL intensities.

Two pathways for nonlinear photon absorption are usually distinguished. In one, the photons might be considered to be absorbed 'sequentially' in time with the first photon leaving the ion in a stationary state and the second photon 'later' removing the second electron via photoionization of the ion. Obviously, this can only happen if the photon energy $E_\gamma = \hbar\omega$ exceeds the ionization potential of the ion I_P^+. At lower photon energies, but under the condition that two photons carry more energy than the sum of the ionization potentials of the neutral and the ion ($I_P + I_P^+$), the removal of two electrons is still possible by quasi-simultaneous (sometimes also referred to as direct or 'non-sequential') absorption (NSDI) of the two photons. In this case, no stationary state of a singly charged ion is involved in the process.

For the reasons mentioned above, triggered by pioneering experiments at FLASH as well as at HH sources [5]–[10], and complicated by the intriguing challenges encountered even for the most simple of such situations, the removal of two electrons from He or Ne by two

photons, theoretical interest has grown rapidly within the last two years (e.g. [11]–[31]). Many of the earlier studies concentrated on evaluation of the total cross section for two-photon double ionization (TPDI) (see, e.g., [29] for a recent compilation of the theoretical results) and the wide range of values obtained by different investigators has led to considerable speculation about the proper treatment of electron correlation in the various theoretical treatments. It now appears that the numerical approximations made using either time-independent or time-dependent descriptions of the process were more to blame for the large disagreement found in the total cross section than were the various levels at which electron correlation was included. Two of the most recent theoretical treatments [22, 32, 33], based on solving the time-dependent Schrödinger equation (TDSE) without approximation on a numerical grid and hence treating electron correlation essentially exactly, have produced total cross sections that are in close agreement. Moreover, these recent treatments yield fully differential distributions for double ionization that are in good mutual accord and are therefore best suited for making comparisons with the current experiments.

In order to trace electron correlation in detail, the coincident detection of the outgoing electrons, ultimately in a kinematically complete experiment, would be most desirable. However, for repetition rates at present achieved at FLASH, even though exceeding those of available HH sources that deliver sufficiently intense EUV radiation, such an experiment is not feasible for NSDI of He (but has been demonstrated for sequential double ionization of Ne [8]). The sum of the momenta of the two photoelectrons produced in NSDI, which depends on the angles of ejection and therefore on the underlying two-electron probability distribution, provides an indirect measure of electron energy sharing and angular correlation. It can be measured via the ion recoil momentum, side-stepping the need for electron detection entirely, and results for Ne and for He, the latter with limited statistical significance, have been reported earlier [5, 6]. Theoretically it has been shown that He^{2+} momentum distributions ($\vec{P}(He^{2+})$) change significantly with the photon energy in the non-sequential regime due to the strongly varying nature of the electron–electron interaction. Independent of the photon energy, the electrons are always emitted at large relative angles with respect to one another, leading to a suppression of high recoil momenta. For energies not too far above the DI threshold at 39.5 eV, the probability distribution in energy sharing is relatively flat, leading to a broad maximum in the $\vec{P}(He^{2+})$ spectra centred at zero momentum (see [6, 34, 35]). At higher energies approaching the sequential threshold at 54.4 eV, the electrons show a propensity towards increasingly unequal energy sharing. This was predicted by some of the present investigators in time-independent calculations and has been dubbed 'virtual sequential ionization' [12, 19, 20]. In the following, 'virtual sequential ionization' refers only to this propensity towards unequal energy sharing and is not meant to imply an uncorrelated angular emission pattern of the two electrons. As one of the electrons obtains a significantly larger momentum than the second one, the recoil ion momentum distribution is also peaked at high momenta. In the earliest theoretical calculations by one of the groups, it was necessary to perform extrapolations from complex to real energies to obtain physically meaningful results. Subsequently, more accurate time-dependent calculations confirmed the qualitative findings of the earlier studies, but differed in their quantitative predictions for photon energies above 50 eV [22, 32, 33].

In the present paper, in a combined experimental and theoretical effort, we search for signatures of 'virtual sequential ionization' in He^{2+} momentum distributions obtained at 52 eV photon energy. Moreover, measured differential data are compared with theory and the reason for differences in published theoretical $\vec{P}(He^{2+})$ distributions is discussed. Additionally, we

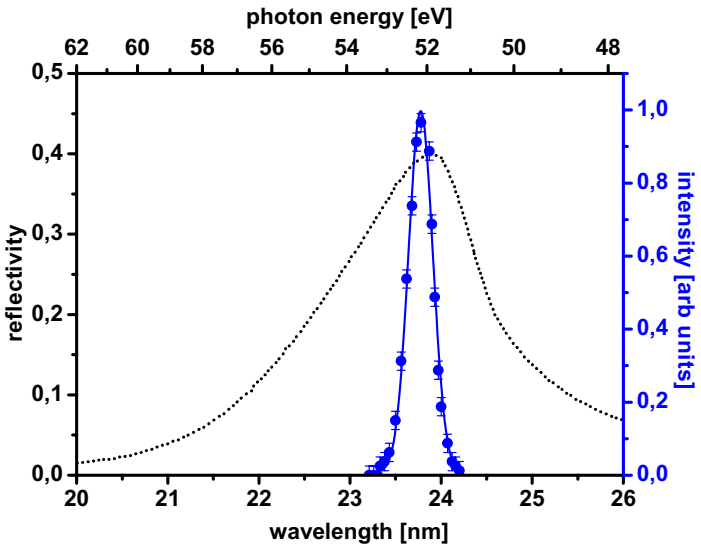

Figure 1. FLASH photon wavelength distribution averaged over several 100 shots. Blue circles: measured data. Full blue curve: Gaussian fit to the data in order to estimate extensions of the wings of the spectra (see text). Dotted black curve: reflection curve of a multilayer mirror in comparison with the measured wavelengths spectrum.

analyse the electron dynamics to show that the recoil ion momentum distributions can be used to extract information about correlated electron emission.

The paper is organized as follows. Section 2 describes the experimental method including a detailed discussion of the momentum resolution achieved. Two theoretical calculations, both solving the TDSE, are briefly sketched in section 3. In section 4, the experimental and theoretical results are presented along with a detailed discussion of small but visible differences between experiment and theory, ending with a brief summary and a view into the future in section 5.

2. Experimental method and momentum resolution

The experiments were performed at the 'unfocussed beamline' (BL3) at the FEL in Hamburg, FLASH [1]. At a 5 Hz pulse train repetition rate, each one containing a train of 30 individual pulses spaced by 10 μs, we had an effective photon pulse rate of 150 Hz at a nominal photon energy of 52 eV. Due to the SASE (self-amplified spontaneous emission; [36]) nature of the radiation from FLASH, the pulse properties show statistical fluctuations from shot to shot (see, e.g., [37]), and recent auto-correlation [38, 39], THz streaking [40] and earlier indirect spectroscopic measurements indicate, in agreement with SASE simulation calculations [37], that up to three longitudinal modes are present, depending on the actual setting of the machine. Averaging over 30 or 100 shots, respectively, a rather broad spectrum is obtained for the present experiment, centred at 52 eV with a full-width at half-maximum (FWHM) of < 1 eV, as shown in figure 1 (blue circles).

The unfocused beam traverses the spectrometer, a many-particle electron and ion momentum imaging system (reaction microscope, REMI) sketched in figure 2. It is then reflected by a split (to allow for VUV–VUV pump-probe) multi-layer mirror with a maximum reflectivity of 40% peaked at 51.9 eV (23.9 nm) with an FWHM of 4.5 eV [41], such that

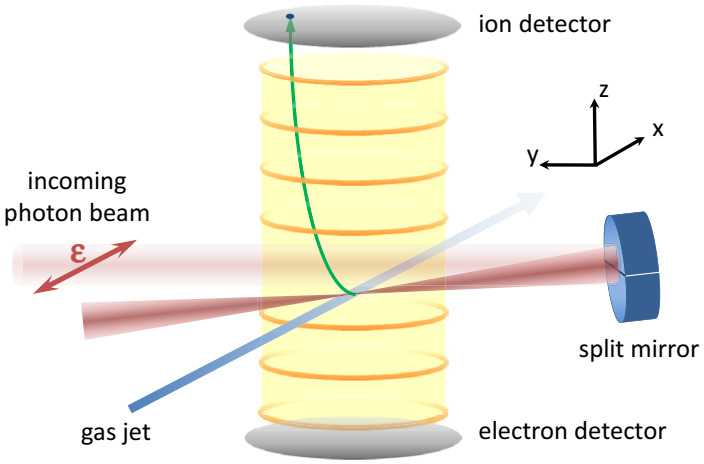

Figure 2. Sketch of the experimental REMI setup.

higher order harmonic radiation from the FEL is efficiently suppressed to a negligibly low level. Moreover, high-energy wings possibly exceeding 54 eV are further reduced by the reflectivity characteristics of the mirror. Fitting a Gaussian to the measured part of the spectrum (blue line in figure 1) and folding it with the mirror reflectivity, we estimate that the maximum relative contribution of radiation with $\hbar\omega \geqslant 54$ eV is below 10^{-10} and, thus, negligible. With a focus diameter of $\sim$10 μm and single pulse energies of a few μJ at a pulse duration of $\sim$30 fs, peak intensities of I $\cong 10^{13}$–10^{14} W cm^{-2} were reached. The focus diameter was estimated by moving the two halves of the split mirror with respect to each other, thereby producing two separate foci in the target and scanning the spatial overlap function by inspecting a nonlinear signal.

The focused light beam intersects a well-collimated (1.0 mm diameter) and intrinsically cold supersonic He gas jet propagating transverse to the photon beam direction at a density of about 10^9 atoms cm^{-3}. The pressure before expansion was 2 bar and the 30 μm nozzle was cooled to 20 K in order to reduce the internal temperature of the atoms for optimized momentum resolution. He^+ and He^{2+} fragments were projected by means of an electric field (2 V cm^{-1}) onto a time- and position-sensitive micro-channel plate (MCP) detector (diameter 120 mm, position resolution 0.1 mm, delay-line read-out). From the measured time-of-flight (TOF) and position of each individual ion, the initial three-dimensional (3D) momentum vectors were reconstructed. In principle, the apparatus, a fully equipped REMI, is capable of measuring the momenta of emitted electrons as well by projecting them via combined electric and magnetic fields on a detector opposite to the ion MCP, as indicated in figure 2. However, due to the large number of electrons emerging from single ionization with ionization yields exceeding those for TPDI by more than three orders of magnitude [42], and due to the small count rate of true He^{2+} events (enforced to reduce the influence of space charge effects on the momentum measurements, as discussed later), no meaningful coincident electron spectra could be recorded. This will only become feasible at significantly enhanced FLASH repetition rates.

Considerable care has been taken to characterize the momentum resolution achieved. In order to measure the intrinsic spectrometer resolution, we have attenuated the incoming beam by many orders of magnitude (using a combination of slits and a gas attenuator) and measured under clean conditions the momentum distribution of singly charged ions shown in figure 3(a). Here, less than one He^+ ion was produced per pulse, so space charge effects in the target area and saturation of the detector can be completely neglected. From a cut through the 3D momentum

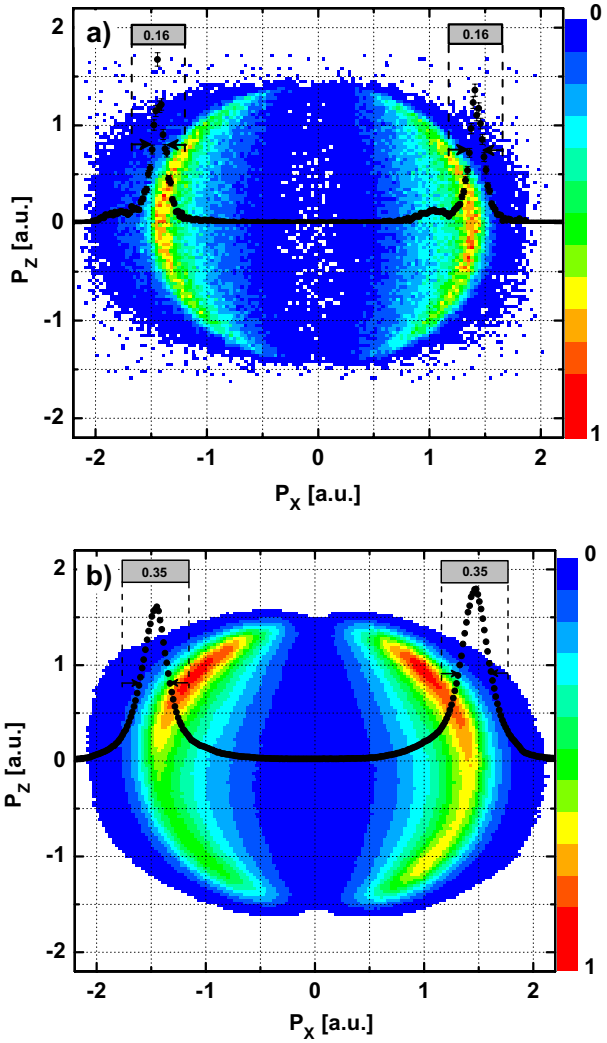

Figure 3. He^{1+} momentum distribution in two dimensions (x and z, see figure 2) at low (a) and high (b) intensity (see text) integrated over P_y. Black dotted curves: projections for $|P_z| < 0.3$ a.u.

distribution (superimposed curve in figure 3(a)), we obtain an FWHM of ∼0.2 a.u. in reasonable agreement with the expected temperature for the He atoms in the jet under present expansion conditions. In addition to the expected momentum peaks, we observe small but clearly visible sub-structures that are shifted towards more negative P_x with respect to the main peaks. They arise for single ionization because the FEL beam passes the target twice, unfocused on its way in and focused when back-reflected. The two beams hit the target at slightly different positions and ionization by the incoming part leads to the faint and shifted image on the detector. This contribution is essentially absent for He double ionization which only occurs with significant probability at high intensities, i.e. in the focused part of the beam. Therefore, in order to achieve reasonable statistical evidence within available beamtimes, we have used the unattenuated beam, which then resulted in significantly enhanced He^+ ion rates of about 25 detected ions per pulse.

Inspecting the $\vec{P}(He^+)$ spectrum in figure 3(b) under these conditions, a significant change is visible: it is much broader, exhibiting an FWHM of ∼0.4 a.u. with the maximum slightly

shifted along the x-direction by 0.05 a.u., and it is asymmetric. While the asymmetry is a result of detector saturation, less pronounced at short ion flight times (upper part of the spectrum) and increasingly important for larger TOFs, the broadening of the spectrum and the shift of the maximum are the combined effect of space charge and detector response at saturation. Essentially, it is difficult to disentangle the two contributions, which is unfortunate, since only the former affects the He^{2+} spectra: at the much shorter TOFs when the doubly charged ions arrive at the detector, saturation effects are absent. Nevertheless, we have attempted an educated guess at space-charge broadening. With a one-photon single ionization cross section of $\sigma_{PI} \sim 2 \times 10^{-18}\,cm^2$, 10^{12} photons per pulse and a focal spot area of $8 \times 10^{-7}\,cm^2$ ($10\,\mu m$ diameter), i.e. with $\sim 10^{18}\,photons\,cm^{-2}$, we essentially ionize every target atom in the focus volume. We approximate this volume as a cylinder with radius R and length L, given by the focus and gas jet diameter, respectively, to be $80\,\mu m^2 \times 1000\,\mu m = 8 \times 10^{-8}\,cm^3$. At an estimated target density of $10^9\,cm^{-3}$ (see above), we then produce about $N = 80$ ions per laser shot, which is in reasonable agreement with the number of detected ions of $\sim$25 per shot and a detector efficiency of about 50%. The number of ions due to residual gas ionization is considerably smaller at the given base pressure of 1×10^{-11} mbar. Therefore, for the estimate of the space-charge broadening, we derived an approximate solution of the Laplace equation for this geometry (N ions homogeneously distributed in a cylinder with length $L = 1$ mm and radius $R = 5\,\mu m$) and calculated, for an ion located at radius r, the potential energy that is eventually converted into kinetic energy due to Coulomb repulsion $E(r) = (Ne^2/L) \cdot (r/R)^2 \cdot \ln(L/r)$. For the present conditions ($N = 50$), the estimated maximum kinetic energy that ions gain when starting at the edge ($r = R$) of the cylinder is $E_{max} \approx 0.3$ meV or, correspondingly, the He^+ ions obtain a maximum change in momentum of $p_{max} \approx 0.4$ a.u. in the direction transverse to the FEL beam axis. Along the beam axis a much smaller net momentum is transferred, actually decreasing to zero for an infinitely extended volume or $L \gg R$. Assuming a homogeneous He^+ density in the focal volume, we arrive, after transformation from cylindrical to Cartesian coordinates, at an expected broadening for He^+ ions of about 0.6 a.u. FWHM, slightly larger but in reasonably good agreement with the measured FWHM of 0.4 a.u. (high intensity). Doubly charged ions that are created dominantly in the inner part of the focus due to the quadratic intensity dependence of the TPDI cross section can now be placed in the He^+ ion cloud with a Gaussian distribution function exhibiting a diameter of only $\sim 7\,\mu m$ FWHM. Performing the same calculation, we arrive at a Gaussian-shaped broadening of $\sim$0.8 a.u. FWHM for the He^{2+} momentum components perpendicular to the cylinder axis. Therefore, in the comparison of the experimental results with theory, this transverse (with respect to the FEL beam propagation) broadening was taken into account by folding the theoretical results accordingly.

For the above reasons, the target density was reduced as much as possible to still obtain a reasonable signal-to-background ratio. However, the background level, mainly due to ionization of H_2 molecules, which are not distinguishable from He^{2+} in the TOF spectra alone due to the identical charge-to-mass ratio, is significant (on the level of 30–40%) and has to be subtracted carefully. The H_2^+ ions that emerge from residual gas ionization are created not only in the focal volume (intersection of FEL beam and gas jet) but also along the whole FEL beam trajectory with typical kinetic energies of 25 meV (300 K room temperature motion). As a result, their momentum distribution in all spatial directions is much broader compared to those of the He^{2+} events, such that a linear fit to the H_2^+ distribution in each direction outside the location where the true He^{2+} ions occur provides a very precise estimate of the background.

3. Theory

The experimental results are compared with state-of-the-art calculations employing two different theoretical approaches, which are referred to here as the Vienna (V) and Berkeley (B) collaborations. In both approaches the TDSE is solved on a numerical grid, but with different numerical methods and using different techniques for constructing the two-electron momentum distributions from the time-propagated wave packet. Different numerical techniques are also employed in calculating the recoil-ion momentum distributions from the underlying two-electron angular distributions. Since the final $P(\vec{P}(He^{2+}))$ is sensitive to small changes in the joint angular distributions, it was essential to ensure convergence of the latter to obtain reliable values for the former.

Both calculations have been described in the literature such that only the salient features and differences are stressed in this paper. The approach of the V-group (cf [22]) directly solves the TDSE. This is done by expanding the angular coordinates in coupled spherical harmonics (time-dependent close-coupling), and employing a finite-element discrete variable representation (FEDVR) for the radial degrees of freedom [43]. The wave function is then propagated in time using a short iterative Lanczos algorithm [44]. The combination of these techniques allows for an efficient parallel implementation, the speed of which has been shown to scale linearly with the number of processors up to 2000 CPUs. This makes it possible to simulate (long) pulses that closely represent the time structure of the VUV pulses produced by FLASH and to perform extensive convergence tests with respect to all relevant variables [22, 30]. In particular, it has been shown by the V-group that projection onto products of Coulomb waves produces stable and correct results for double ionization, provided that the projection is performed at a time when the electrons are far enough apart. We have tested that we achieve well-converged results for the joint angular, energy and recoil ion momentum distributions in one-photon double ionization near the double ionization threshold [34]. To ensure convergence also for the process discussed here, the same checks were made again for the specific VUV pulses used in this paper, and no change of the recoil-ion momentum distributions was found with larger basis sets when sufficiently long pulses (>11 fs) were used to simulate the experimental conditions (see the discussion below).

The recoil momentum cross section is a derived quantity and can be calculated in different ways. For example, Pont and Shakeshaft [45] show how to derive the recoil cross section from the two-electron momentum distribution by transforming to sum- and relative-momentum (Jacobi) coordinates and integrating over the latter.

In the approach of the V-group, the recoil momentum probability distribution is computed by Monte Carlo techniques to generate a large number of pairs of electron momenta distributed according to the full probability distribution $P_{DI}(\vec{k}_1, \vec{k}_2)$. From the electron momenta, the recoil ion momentum, $\vec{Q} = -\vec{k}_1 - \vec{k}_2$, is computed and used to fill histograms, exactly as done in experiment. The accuracy of this method depends on the number of electron pairs that we generate and the accuracy of the grid on which the probability distribution is calculated. Extensive testing has been performed to ensure that the plots shown in the current paper are converged. As a further test, the generated angular and energy distributions have been compared to the directly calculated distributions and perfect agreement is obtained. Note that the flexibility of this approach enables us to easily generate the probability distribution as a function of *any* coordinates.

In the method employed by the B collaboration [46], the TDSE is also solved with a representation of the time-dependent Hamiltonian in a basis of FEDVR functions defined on an exterior complex-scaled grid. The complex turning points of the grid are chosen large enough that the wave packet remains entirely on the real portion of the grid during the finite length of the pulse. After the pulse stops, the system continues to evolve under the field-free atomic Hamiltonian. The wave packet is then effectively propagated to infinite time by defining a scattered wave corresponding to a specific final energy as the Fourier transform of the time-propagated packet. This scattered wave satisfies a time-independent driven equation that is solved with pure outgoing boundary conditions using exterior complex scaling. The amplitudes for single and double ionization are then extracted using surface integrals involving the scattered wave and testing functions appropriate for the process under consideration. By fixing the final state energy, this procedure, as we have shown [32], has the attractive feature of allowing amplitudes to be extracted over the entire range of energies within the bandwidth of the pulse. Provided that there are no intermediate resonances that fall within the bandwidth of the pulse and provided that the fields are such that photoejection can be described by lowest-order time-dependent perturbation theory, this procedure gives an unambiguous prescription for calculating the generalized cross sections for single and double ionization. In the present context, the sequential process acts like an intermediate resonance and the pulse bandwidth must be such that there are no significant contributions above the sequential threshold at 54.4 eV, where the generalized TPDI cross section is no longer defined.

The B collaboration calculates the recoil ion momentum cross section from the triple differential cross sections for TPDI by direct numerical integration over all ejection angles of the two photoelectrons that lead to a specified total momentum. The numerical implementation requires some care, since the ranges in the directions of ejection that can lead to a specified total momentum are finite and change with energy sharing between the electrons. The numerical algorithm used is described in some detail in [20].

4. Results and discussion

In figure 4, experimental and theoretical results for the recoil-ion momentum distribution along the polarization axis (x-direction) are shown, either integrating over the complete (figure 4(a)), or only over a smaller part (figure 4(b)) of the, transverse (with respect to the polarization) momentum distribution. The V calculations used an 11 fs sine-squared pulse with a mean energy of 52 eV and include all double ionization events when constructing the ion recoil distributions. We checked that a 20 fs sine-squared pulse produces almost exactly the same recoil distribution. The results shown below are obtained from the 11 fs pulse, which has a bandwidth (FWHM) of 0.4 eV, similar to the averaged spectral width of the FLASH pulses. The B calculations used a 52 eV 2 fs pulse (FWHM = 2.1 eV) but only used pairs of photoelectrons with a total energy of $(2 \times 52–78.99)$ eV to construct the ion recoil distributions. This corresponds to choosing those electrons that are produced by 52 eV photons if the spectral broadening in the intermediate step is neglected. The two calculations are in general agreement with each other and only minor differences can be found. The complete distributions (figure 4(a)) exhibit two maxima at about ± 0.9 a.u. The ratio between these maxima and the local minimum at 0 a.u. is slightly higher for the B calculation, due to the larger spectral bandwidth of the 2 fs pulse. This pulse samples processes closer to the sequential threshold, where the energy sharing is more extreme. The maxima persist in the distribution restricted in the transverse direction (figure 4(b)) by selecting

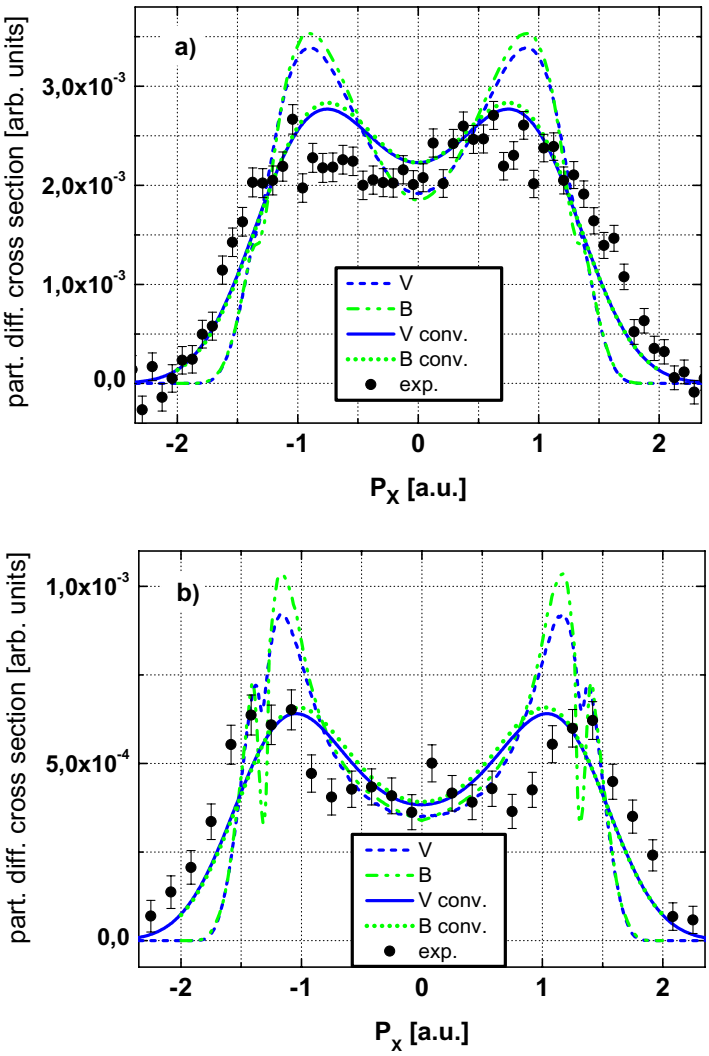

Figure 4. (a) Longitudinal momentum distribution of He^{2+} integrated over the two other momentum components. Black circles: experimental data. Lines: theoretical results before and after convolution with the experimental resolution (FWHM = 0.8 a.u., see text). (b) The same as (a) but integrated over $|P_y|, |P_z| < 0.3$ a.u.

only events with $|P_y|$, $|P_z| < 0.3$ a.u. Here, the maxima are shifted along the polarization direction to about 1.25 a.u, close to the value of the ion recoil momentum when one electron carries all the available energy, $P_{||}^{\max} = \sqrt{2(2\hbar\omega - I_P^+ - I_P^{2+})} \sim 1.35$ a.u. (for a photon energy of 52 eV). Additionally, each maximum is split up into two individual peaks with the respective sub-peak at higher absolute momentum being distinctly smaller. In essence, both calculations show that, in the non-sequential regime, the electrons are preferentially emitted in a back-to-back configuration, while ejection in the same direction is strongly suppressed. At the same time, the energy distribution of the two electrons is peaked at extreme energy sharing, where one electron receives most of the available energy, whereas the second one gets little energy and momentum. This leads to the existence of the main maximum along the polarization direction.

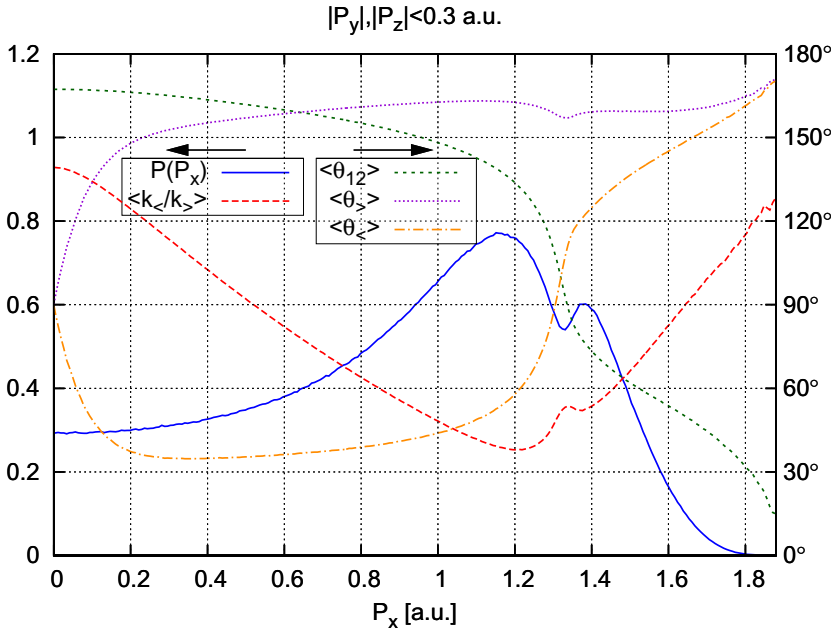

Figure 5. Theoretical results (obtained from the V-calculation) for the distribution of recoil momentum in the longitudinal direction P_x, restricted to small transverse momenta ($|P_y|, |P_z| < 0.3$ a.u.). In addition, we show the expectation values for the electrons contributing to each value of the recoil momentum. The values shown are the ratio between the momenta of the slower and the faster electron, $\langle k_</k_> \rangle$, the relative angle between the two electrons, $\langle \theta_{12} \rangle$, and the angle between the polarization axis and the slower (faster) electron, $\langle \theta_< \rangle$ ($\langle \theta_> \rangle$). As indicated by the arrows, the distribution in P_x (in arbitrary units) and the ratio of momenta are on the left axis, whereas angles are shown on the right axis.

The splitting of the maxima can be understood from the emission patterns of the electrons contributing to each given recoil momentum. We analyse this by exploiting the flexibility of the Monte Carlo algorithm used by the V collaboration to show different expectation values for all electrons contributing to a specific longitudinal recoil momentum (with restricted transverse momenta). Figure 5 shows the relative angle between the two electrons, $\langle \theta_{12} \rangle$, the angle between each of the electrons and the polarization axis, $\langle \theta_i \rangle$, and the ratio between the momenta of the slower and the faster electron, $\langle k_</k_> \rangle$, all as a function of the longitudinal recoil momentum P_x. As predicted, the peak of the recoil momentum distribution stems from contributions with strongly asymmetric momentum sharing, where the slow electron is about four times slower than the fast one. In addition, figure 5 reveals that, for $P_x > 0.2$ a.u., the faster electron is always emitted close to the polarization axis. In contrast, the angle of the slower electron relative to the polarization axis and, consequently, the angle between the electrons depend strongly on P_x. The low-momentum peak in the double-peak structure comes from configurations where the slow electron is emitted in almost the opposite direction to the fast electron, with an average relative angle of about 135°. The smaller peak at higher recoil momenta comes from electrons emitted into the same hemisphere. However, the average relative angle is still larger than 70°, while emission at even smaller relative angles is strongly suppressed because of the Coulomb repulsion between the electrons. Recoil momenta close to the dip at $P_x = 1.35$ a.u. are reached when the electrons are emitted at right angles to each other. As the fast electron is emitted

close to the polarization axis, this configuration corresponds to emission of the slower electron at right angles to the polarization axis. It has been shown previously [22, 47] that the node line of the single-photon Hertz dipole pattern at a 90° emission angle survives even in strongly correlated TPDI processes, indicative of absorption of one photon by each electron. This strong suppression of emission at right angles to the polarization axis is responsible for the dip in the recoil ion momentum distribution and thus the splitting of the peak.

The splitting of the main maximum has previously been [19, 20, 33] discussed by the B collaboration in terms of virtual sequential ionization. The earlier time-independent calculations [19, 20] showed this feature even more distinctly, even in the recoil distributions without restriction of transverse momenta. The recently published results of time-dependent calculations [33] have pointed to intrinsic numerical error in the extrapolation from complex values of photon energy required in the earlier calculations that implicitly sample the energy region above the sequential threshold, resulting in an overestimation of electron ejection at small relative angles. The present double peak structure in the longitudinal momentum distribution is therefore only visible for cuts in the transverse momentum distribution at small values ($|P_y|, |P_z| < 0.3$ a.u.) and disappears for unrestricted transverse momenta.

In figure 4, both theoretical distributions, convoluted with the experimental resolution taking into account the effect of space-charge broadening, are compared to the experimental results. Since no absolute experimental cross sections were recorded, we have normalized experimental as well as theoretical results such that the integral over P_x in figure 4(a) resembling the total cross section for TPDI of He gives one. Note that this normalization is maintained for all other distributions and doubly differential cross sections, such that they are relatively normalized to each other. In general, we find good agreement and the predicted peak structure is clearly visible for the first time. This proves the existence of 'virtual sequential ionization' favouring the asymmetric energy sharing with one fast and one slow electron being emitted, due to electron–electron repulsion, mainly in opposite directions. Unfortunately, mainly as an effect of the unavoidable (with the present FEL repetition rate) broadening of the spectrum due to space charge generated by the He^{1+} ions in the focal volume, the peak splitting visible in both calculations with restricted transverse momenta ($|P_y|, |P_z| < 0.3$ a.u., figure 4(b)) is essentially washed out in the measurement such that we are not in a position to experimentally benchmark the prediction of this feature.

While the position of the experimental maxima is in reasonable agreement with the theoretical prediction for the complete distribution (figure 4(a)), they seem to be slightly shifted towards larger values in the restricted one (figure 4(b)). Exploiting the mirror symmetry with respect to the plane $P_x = 0$ a.u., we can sum contributions with $P_x < 0$ and $P_x > 0$ by plotting the momentum distribution as a function of $|P_x|$ in figure 6 and thus reduce the statistical uncertainty of the data without any loss of information. Now small but significant differences between experimental and theoretical results become more apparent. In both calculations, the peak is more pronounced than found experimentally for the full (figure 6(a)) distribution, with minor differences between the two predictions becoming more clearly visible. Moreover, in the complete as well as in the restricted spectra (figure 6(b)), we find more intensity in the experimental data at larger momenta close to the second, outer maximum of both calculations.

Before discussing the possible reasons for this discrepancy, we further elaborate on the influence of the space charge by inspecting first changes between low- and high-intensity data for singly charged helium. Applying identical cuts to these data, a shift in the peak position of 0.05 a.u. towards larger momenta was found (see superimposed curves in figure 3) while going

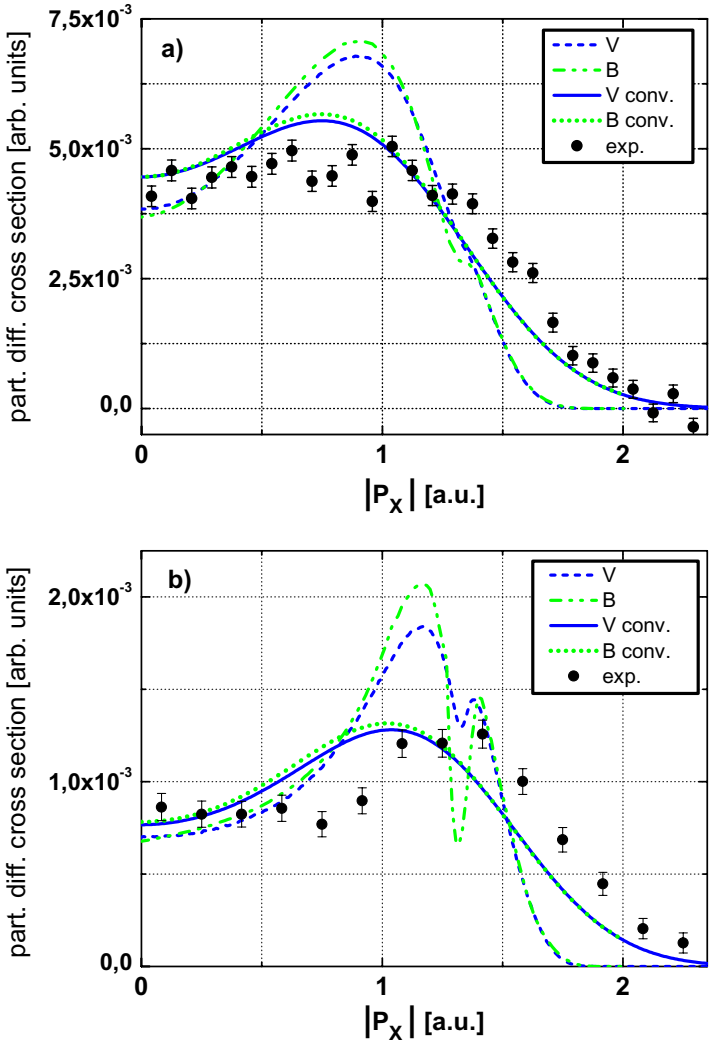

Figure 6. The same as figure 4 but adding the experimental data for $P_x < 0$ and $P_x > 0$ in order to decrease the statistical error of the mirror symmetric distribution.

from low to high FEL intensities. Assuming similar behaviour for the doubly charged He^{2+} ions, we expect a corresponding shift of 0.07 a.u., which is significantly less than the observed offset of ∼0.25 a.u. Moreover, in figure 7 we have plotted the corresponding distributions along the P_y and P_z axes, for which we expect a different influence of the space-charge broadening. Whereas it influences the P_z-direction, it should essentially be absent along P_y, the beam propagation direction, assuming $L \gg R$ as given in the experiment. Indeed, the calculated unfolded V spectrum (and the virtually identical B result) agrees very well with the experimental spectrum as a function of $|P_y|$, being significantly less broad than the corresponding $|P_z|$ spectrum, which itself is in good accordance with the folded theoretical distribution. This shows, within error bars, that we do have a space-charge influence and proves that its magnitude is consistent with our previous estimates. The upper limit consistent with the data would be folding the theoretical distribution with an FWHM of 0.9 a.u. Even doing so for the x-distributions, we still find disagreement between experiment and both calculations.

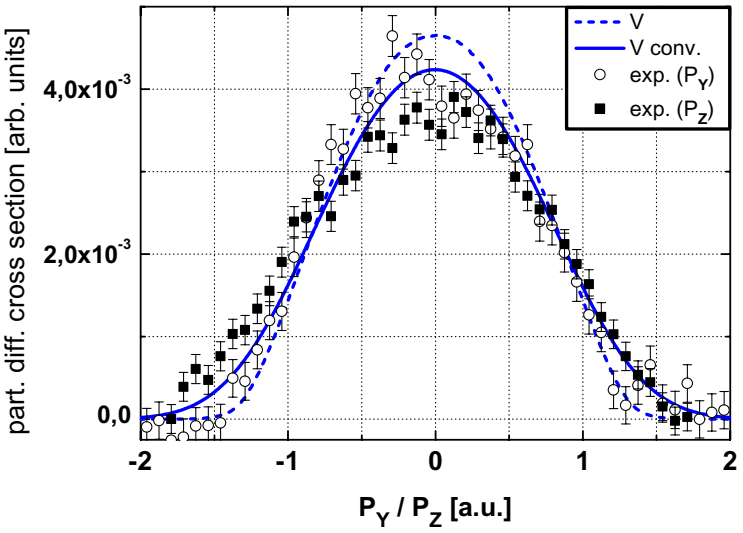

Figure 7. Transverse momentum spectra along the z- (full squares) and y- (open circles) directions in comparison with the V prediction (representing both theories), unfolded (dashed line) and folded with the experimental resolution (full line).

We are thus left with the finding that both the complete and the restricted experimental distributions are systematically above the calculations in the momentum region between ± 1.25 and ± 1.75 a.u. Moreover, the peak-to-minimum ratio in figure 6(a) and the position of the peak (figure 6(b)) differ outside statistical error bars. Other experimental effects that might lead to such deviations, like the contribution of HH radiation or contributions in the spectrum extending above 54 eV, can be safely ignored, as discussed before. Uncertainties in the background subtraction might overestimate higher momentum components, which become visible in small asymmetries in figures 4(a) and (b). Taking this asymmetry as the maximum respective error, we still cannot explain the observed deviations.

At the present point, we can only speculate about potential reasons. One possibility might be a larger contribution of emission of the two electrons into the same hemisphere, which would, consequently, result in a shift in the maximum position. Essentially, this effect is represented in the high-momentum shoulder (figure 6(a)) or peak (figure 6(b)) in theory, and comparison with experiment would imply that theory underestimates this contribution being equivalent to an overestimation of the electron–electron repulsion in the final state. This appears unlikely, since the repulsion is actually neglected for the projection at asymptotic distances used by the V collaboration, which gives nearly perfect agreement with the ECS approach of the B group. Still, we would like to note that an increased probability of ejection at small relative angles in the theoretical results (see figures 5 and 6(b)) would result in significantly improved agreement with the experiment. It is also worth noting that the theoretical calculations show that the relative contribution of the high-momentum peak is very sensitive to photon energy and increases substantially if the photon energy is increased above 52 eV, so that even a small uncertainty in photon energy could have a big effect. Certainly, remaining background contributions on the high-momentum side cannot be completely ruled out, whereas 'missing' intensity on the low-momentum side of the peak can hardly be understood in terms of experimental uncertainties or by spurious potential contributions at higher photon energies.

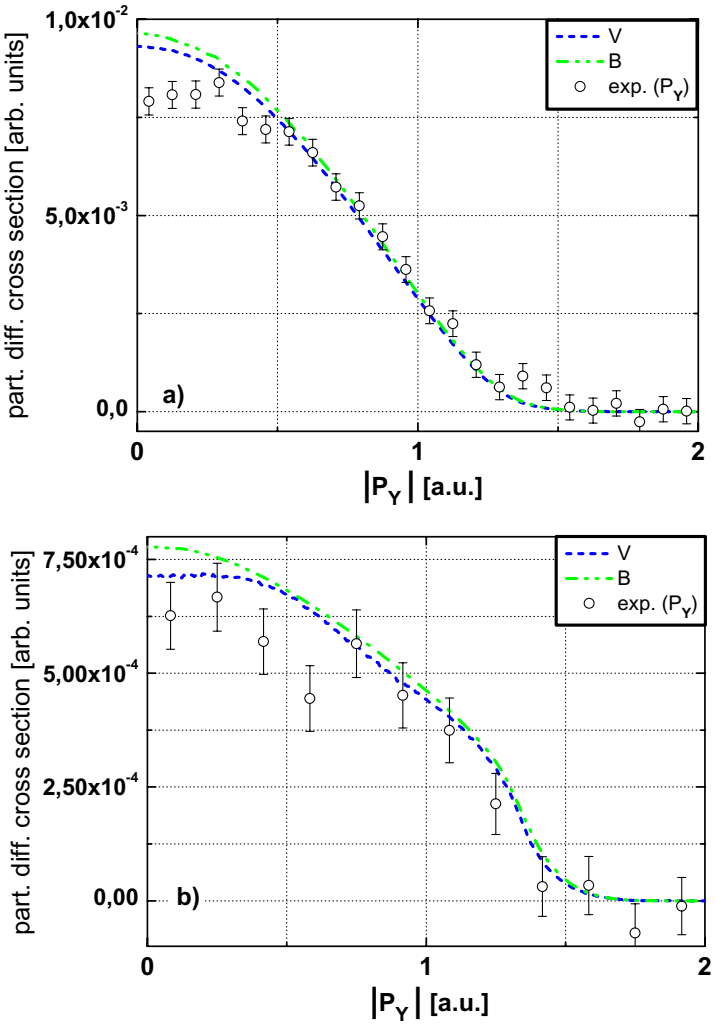

Figure 8. Momentum spectra along the y-direction (unaffected by space-charge broadening) adding data for $P_y < 0$ and $P_y > 0$. (a) Integrated over the other two momentum components and (b) integrated over restricted momenta $|P_x|$, $|P_z| < 0.3$ a.u. only. Lines: unfolded theoretical results as indicated.

To further shed light on the dynamics of TPDI in helium, figure 8 depicts the momentum distribution transverse to the polarization direction along the y-direction (essentially unaffected by space-charge broadening), with (figure 8(b)) and without (figure 8(a)) the transverse restriction, as in the previous plots. These cuts are rather insensitive to pulse length effects, such that both calculations show almost identical behaviour with only minor differences at small momenta.

5. Summary and view into the future

In summary, we have presented differential measurements on non-sequential TPDI of He at a photon energy of 52 eV, and compared them with two state-of-the-art calculations, both solving the TDSE. We find the first experimental evidence for virtual sequential ionization

showing that, close to the threshold for sequential TPDI, the energy sharing between the two emitted electrons is predominantly asymmetric. We have presented a detailed analysis of the origin of the peak splitting observed in the distribution in longitudinal momentum (restricted to small transverse momenta), showing the signature of strongly correlated electron emission in recoil ion momentum distributions. Generally, the observed momentum distributions are in good agreement with the theoretical predictions, with the exception of a slight but nevertheless significant discrepancy in the longitudinal direction, where we find the maximum position of the experimental momentum distribution shifted towards larger momenta. The origin of this discrepancy remains, at present, unexplained.

In the future, with the update of FLASH and the related increase in repetition rate, we envision being able to record fully differential cross sections, thus providing the ultimate benchmark data for advancing theory.

Acknowledgments

The authors are greatly indebted to the scientific and technical team at FLASH, in particular, the machine operators and run coordinators, striving for optimal beamtime conditions. Support from the Max-Planck Advanced Study Group at CFEL is gratefully acknowledged. YHJ acknowledges support from DFG project no. JI 110/2-1. Work at LBNL was performed under the auspices of the US DOE and supported by the OBES, Division of Chemical Sciences under contract no. DE-AC02-05CH11231. CWM acknowledges support from the NSF (grant no. PHY-0604628). The V team acknowledges support from the NSF TeraGrid computational facilities at the Texas Advanced Computing Center (TACC) and at the National Institute for Computational Science (NICS), and institutional computing resources at Los Alamos National Laboratory for computer time to perform the computations. Work at Vienna University of Technology was supported by the FWF-Austria (grant no. SFB016). JF acknowledges support from the NSF through a grant to ITAMP. OH, ML and MFK acknowledge support from the DFG via the Emmy-Noether programme and the Cluster of Excellence: Munich Centre for Advanced Photonics.

References

[1] Ackermann W *et al* 2007 *Nat. Photonics* **1** 336
[2] Shintake T *et al* 2008 *Nat. Photonics* **2** 555
[3] Emma P *et al* 2009 First lasing of the LCLS x-ray FEL at 1.5 Å *Proc. PAC09* Available at: www.jacow.org
[4] Krausz F and Ivanov M 2009 *Rev. Mod. Phys.* **81** 163
[5] Moshammer R *et al* 2007 *Phys. Rev. Lett.* **98** 203001
[6] Rudenko A *et al* 2008 *Phys. Rev. Lett.* **101** 073003
[7] Jiang Y H *et al* 2009 *J. Phys. B: At. Mol. Phys.* **42** 134012
[8] Kurka M *et al* 2009 *J. Phys. B: At. Mol. Phys.* **42** 141002
[9] Sorokin A A, Wellhöfer M, Bobashev S V, Tiedtke K and Richter M 2007 *Phys. Rev.* A **75** 051402
[10] Nabekawa Y, Hasegawa H, Takahashi E J and Midorikawa K 2005 *Phys. Rev. Lett.* **94** 043001
[11] Pronin E A, Manakov N L, Marmo S I and Starace A F 2007 *J. Phys. B : At. Mol. Phys.* **40** 3115
[12] Horner D A, Morales F, Rescigno T N, Martin F and McCurdy C W 2007 *Phys. Rev.* A **76** 030701
[13] Shakeshaft R 2007 *Phys. Rev.* A **76** 063405
[14] Pindzola M *et al* 2007 *J. Phys. B: At. Mol. Phys.* **40** R39
[15] Kheifets A S 2007 *J. Phys. B: At. Mol. Phys.* **40** F313

[16] Nikolopoulos L A A and Lambropoulos P 2007 *J. Phys. B: At. Mol. Phys.* **40** 1347
[17] Ivanov I A and Kheifets A S 2007 *Phys. Rev.* A **75** 033411
[18] Kheifets A S, Ivanov I A and Bray I 2007 *Phys. Rev.* A **75** 024702
[19] Horner D A, Rescigno T N and McCurdy C W 2008 *Phys. Rev.* A **77** 030703
[20] Horner D A, McCurdy C W and Rescigno T N 2008 *Phys. Rev.* A **78** 043416
[21] Hamonou L, van der Hart H W, Dunseath K M and Terao-Dunseath M 2008 *J. Phys. B: At. Mol. Phys.* **41** 015603
[22] Feist J, Nagele S, Pazourek R, Persson E, Schneider B I, Collins L A and Burgdörfer J 2008 *Phys. Rev.* A **77** 043420
[23] Guan X, Bartschat K and Schneider B I 2008 *Phys. Rev.* A **77** 043421
[24] Foumouo E, Antoine P, Bachau H and Piraux B 2008 *New J. Phys.* **10** 025017
[25] Lambropoulos P and Nikolopoulos L A A 2008 *New J. Phys.* **10** 025012
[26] Foumouo E, Antoine P, Piraux B, Malegat L, Bachau H and Shakeshaft R 2008 *J. Phys. B: At. Mol. Phys.* **41** 051001
[27] Makris M G and Lambropoulos P 2008 *Phys. Rev.* A **77** 023401
[28] Makris M G and Lambropoulos P 2008 *Phys. Rev.* A **77** 023415
[29] Antoine P, Foumouo E, Piraux B, Shimizu T, Hasegawa H, Nabekawa Y and Midorikawa K 2008 *Phys. Rev.* A **78** 023415
[30] Feist J, Pazourek R, Nagele S, Persson E, Schneider B I, Collins L A and Burgdörfer J 2009 *J. Phys. B: At. Mol. Phys.* **42** 134014
[31] Fritzsche S, Grum-Grzhimailo A N, Gryzlova E V and Kabachnik N M 2008 *J. Phys. B: At. Mol. Phys.* **41** 165601
[32] Palacios A, Rescigno T N and McCurdy C W 2009 *Phys. Rev.* A **79** 033402
[33] Horner D A, Rescigno T N and McCurdy C W 2010 *Phys. Rev.* A **81** 023410
[34] Pazourek R 2008 *Master's Thesis* Vienna University of Technology
[35] Feist J 2009 *PhD Thesis* Vienna University of Technology
[36] Ayvazyan V *et al* 2002 *Eur. Phys. J.* D **20** 149
[37] Saldin E L, Schneidmiller E A and Yurkov M V 2006 *Nucl. Instrum. Methods* B **562** 472
[38] Mitzner R *et al* 2009 *Phys. Rev.* A **80** 025402
[39] Schlotter W F, Sorgenfrei F, Beeck T, Beye M, Gieschen S, Meyer H, Nagasono M, Föhlisch A and Wurth W 2010 *Opt. Lett.* **35** 372
[40] Frühling U *et al* 2009 *Nat. Photonics* **3** 523
[41] Feigl T 2009 IOF Jena private communication
[42] Nikolopoulos L A A and Lambropoulos P 2006 *J. Phys. B: At. Mol. Phys.* **39** 883
[43] Schneider B I and Collins L A 2005 *J. Non-Cryst. Solids* **351** 1551
[44] Park T J and Light J C 1986 *J. Chem. Phys.* **85** 5870
[45] Pont M and Shakeshaft R 1996 *Phys. Rev.* A **54** 1448
[46] Palacios A, Rescigno T N and McCurdy C W 2007 *Phys. Rev.* A **76** 043420
Palacios A, Rescigno T N and McCurdy C W 2008 *Phys. Rev.* A **77** 032716
[47] Feist J, Nagele S, Pazourek R, Persson E, Schneider B I, Collins L A and Burgdörfer J 2009 *Phys. Rev. Lett.* **103** 063002